Performance Evaluation of Magnetic Resonance Coupling Method for Intra-Body Network (IBNet)

Sayemul Islam[1†], Rajpreet Kaur Gulati[2†], Michael Domic[1], Amitangshu Pal[3], Krishna Kant[2], Albert Kim[1]

***Abstract*— Effective management of emerging medical devices can lead to new insights in healthcare. Thus, human body communication (HBC) is becoming increasingly important. In this paper, we present magnetic resonance (MR) coupling as a promising method for the intra-body network (IBNet). The study reveals that MR coupling can effectively send or receive signals in biological tissue, with a maximum path loss of PL $\leq$ 33 dB (i.e. at 13.56 MHz), which is lower than other methods (e.g., galvanic, capacitive, or RF) for the same distance (d = 100 cm). The angular orientation of the transmitter and receiver coils at short and long distances also show a minor variation of the path loss (0.19 $\leq \Delta$PL $\leq$ 0.62 dB), but more dependency on the distance (0.0547 dB/cm). Additionally, different postures during the MR coupling essentially does not affect path loss (ΔPL $\leq \pm$ 0.21 dB). In the multi-nodal transmission scenario, the MR coupling demonstrates that two nodes can simultaneously receive signals with -16.77 dBm loss at 60 cm and 100 cm distances, respectively. Such multi-node MR transmission can be utilized for communication, sensing, and powering wearable and implantable devices.**

***Index Terms*— Intra-body sensor network, magnetic communication, magnetic resonance coupling, wireless power transfer.**

I. Introduction

Since the evolution of the pacemaker in the 1950s [1], subsequent decades have witnessed a significant development of implantable medical devices due to the advancements in integrated circuits, microelectromechanical systems (MEMS), wireless systems, and battery technologies. Today, these implantable medical devices have led to new insights in ambulatory monitoring and automated diagnosis for many chronic diseases [2], [3]. Briefly, the implantable medical devices (IMDs) can operate in two different modes: (a) monitoring disease related parameters and corresponding automated actuation to deliver medicine or physiological stimulation (i.e., closed feedback systems such as pacemakers, implantable cardiac defibrillators, implantable neurostimulators, etc.), and (b) monitoring physiological health parameters that are used by medical practitioners to recommend specific actions (i.e., change in medication, avoidance of certain foods, etc.). For example, in some chronic diseases or deficiencies in natural function of organs, forming a therapeutic network of multiple sensors and actuators inside the body can enable unprecedented management, e.g., overactive bladder control by a spinal cord neuro-modulator based on the bladder pressure monitoring by an implantable pressure sensor; urine volume monitoring by micro-electrode mediated neural recording [4]–[6]; effective pacemaker control via pH, oxygen, respiration, activity, and drug infusion monitoring [7], [8]; or brain-computer interface via an implantable micro-electrode array (where the number of channels can be more than 100) [9].

In view of long-term and continuous monitoring, effective chronic disease management using implantable medical devices require long-term and continuous operation; thus, an intra-body network (IBNet) is becoming increasingly important, further spurred by the advances in ultra-low-power electronics and communications [10]. Fig. 1 visualizes the proposed IBNet. It consists of multiple therapeutic nodes (e.g., wearable or implantable sensors or actuators) and intermediate nodes (or hubs) for external communication, powering, and data storage.

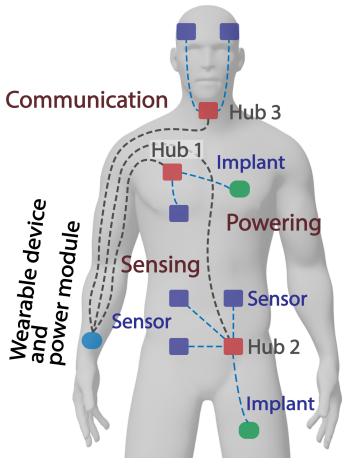

Fig. 1. Illustration of intra-body power/data transmission network.

Although wireless RF technology has been heavily researched [11], [12] for communication and energy transfer, it suffers from poor transmission through biological tissue. It also needs a relatively large antenna, which limits how small the implantable devices can be and prevents implantation in organs such as the brain, heart, and spinal cord without causing significant damage. To overcome the shortcomings

Manuscript submitted July 23, 2021; first revision October 6, 2021; accepted November 16, 2021. "The project was supported by the National Science Foundation grants (ECCS-2029077, CNS-2129659, and CNS-1844944)."

S. Islam, M. Domic and, A. Kim are with the Electrical and Computer Engineering Department, Temple University, Philadelphia, PA 19122 USA. (Corresponding author: Albert Kim, email: albertkim@temple.edu)

R. K. Gulati, and K. Kant are with the Department of Computer and Information Sciences, Temple University, Philadelphia, Pennsylvania 19122 USA. A. Pal, was with Temple University, Philadelphia, PA 19122 USA. He is now with the Computer Science and Engineering Department, Indian Institute of Technology Kanpur, Kanpur, India.

of RF coupling, there are some alternative methods available for intra-body communication. Depending on how the signal is propagated, the methods can be classified into: galvanic coupling (GC) [13], [14], capacitive coupling (CC) [15], [16], magnetic induction/resonance coupling (MI/MR) [17]–[19], or can be a mix of different coupling methods such as combination of capacitive coupling in HBC with MI wireless power transfer (WPT) demonstrated by Zhang et al. [20]. In galvanic coupling (GC), the T_x and R_x electrodes are directly in contact with the skin to induce the communication by means of electric current flow [21]. In capacitive coupling (CC), the signal electrodes create ground capacitance to complete the current loop [15]. In the magnetic resonant (MR) coupling method, the signal is coupled through the body using magnetic coils and magnetic flux [19]. The proposed magnetic resonance coupling is more efficient within biological tissue due to lower path loss achieved by employing the resonating behavior of the coils. It enables transmitting at optimal power to a higher link distance. In this mode of coupling, an electromagnetic signal is coupled into the body using an electromagnetic coil and is tapped from another part of the body using similar coils.

In this paper, we systematically compare three IBNet coupling methods in terms of path loss (section IV-A). We hypothesize that the MR coupling is the most suitable technology for the IBNet since the magnetic permeability of the soft tissue is similar to that for the air [22]. Then, we evaluate different MR coupling combinations (section IV-B). We then systematically evaluate MR coupling in different body parts (section IV-C), angular misalignment between transmitter and receiver (section IV-D), posture change (section IV-E), and multiple receivers modes (section IV-F).

II. Coupling Methods for IBNet

In this section, we briefly review three standard signal coupling methods for IBNet and human body communication (HBC), which are galvanic, capacitive, and magnetic resonance (MR) coupling. Fig. 2 briefly illustrates their working principle.

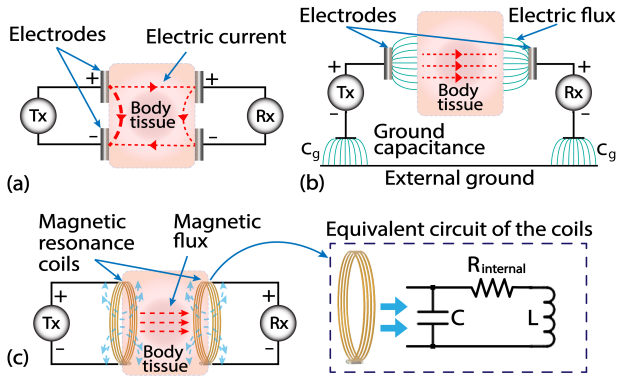

Fig. 2. Intra-body coupling methods: (a) galvanic coupling, (b) capacitive coupling, and (c) magnetic resonance (MR) coupling and equivalent circuit.

A. Galvanic Coupling

The Galvanic HBC is the coupling of the signal to the human body through a pair of electrodes in contact with the skin to be used as a transmitter (T_x) and a receiver (R_x), as shown in Fig. 2(a). When a differential signal is applied, T_x couples the signal to the body by producing a primary current flow and induces galvanic currents (secondary flow) to the R_x. The working mechanism is extensively discussed by Wegmuller et al.; he studies the influence of the electrode size and human body joints on the channel for a stimulus input, based on the position of the T_x and R_x, at different locations on the body [21].

The galvanic coupling is dependent on the current flow through the body. Since only a small fraction of the current goes across the longer path from $T_{x(+)}$ to $R_{x(+)}$ (and back from $R_{x(-)}$ to $T_{x(-)}$), it is generally not an energy efficient coupling method as we show in section IV-A. Furthermore, the relatively low conductivity of the human body may cause rapid signal decays with the distance, resulting in large path loss compared to other approaches [23]. On the positive side, this method does not require an external ground, so it is a reasonably suitable coupling method for wearable and implantable devices.

B. Capacitive Coupling

The capacitive coupling (also known as electrostatic coupling) uses a pair of electrodes as T_x and R_x as shown in Fig. 2(b). The signal electrodes are attached to the body capacitively while the corresponding ground electrodes are left floating, which creates a capacitance with the environment (earth, air, or other objects in the surrounding). The capacitive coupling mechanism can be modeled as distributed RC circuits [24]. Here, the operation frequency is low enough for electrostatic analysis. However, as the frequency is scaled above tens of MHz, the power radiated by electrodes increases. A wave propagation model operating on the surface of a human body was introduced by Bae et al. [25]. In addition, Maity et al. [26] recently introduced a biophysical model where the biophysical parameters (i.e., capacitance, resistance) were estimated for subcutaneous human tissues to explain the complex impedance characteristics of signal transmission using capacitive coupling in the body.

In the capacitive coupling method, the signal flows capacitively through the body and the return signal is propagated through the environment [27]. The capacitive coupling from the on-body into the muscle experiences a significant signal loss, but the signal flow inside the body does not experience much loss and is mostly insensitive to the distance traveled [26]. However, the more recent work suggests substantial and varying “shadowing effects” in various parts of the body [16] leading to higher signal attenuation. These works speak of the “electro-quasistatic” (EQS) effect to describe capacitive coupling operating at frequencies less than 10 MHz. Additionally, due to the weak nature of the received signal and high dependability on the surrounding environment, capacitive coupling in IBNet usually works at a short-range [28] making it unusable for use with implantable/wearable devices at a longer distance.

C. Magnetic Resonance (MR) Coupling

The magnetic resonance coupling refers to the signal coupling between the T_x and R_x coils via magnetic flux as shown in Fig. 2(c). The resonance frequency, which must be identical for transmitter and receiver, is given by $f = 1/2\pi\sqrt{LC}$, where, L is the coil inductance, and C is the capacitance connected in parallel with the coil. The resonance coupling ensures maximum power/signal transfer which also enhances the link distance through the body [19]. The T_x coil generates an oscillating magnetic field that is coupled through the tissue and can be received using an R_x coil placed at other places on the body due to mutual inductance. The current in the T_x coil dictates the mutual inductance (M_{21}) with the R_x coil and can be expressed as, $M_{21} = N_2 \cdot \phi_{21}/I_1$, where N_2 is the number of turns of the R_x coil, and ϕ_{21} is the magnetic flux.

Suppose that the T_x coil has N_1 turns, the current I_1 through the coil generates a magnetic field B_1, and the area covered by the oscillating magnetic field is A_1. If two coils (T_x and R_x) are close to each other, some of the magnetic field lines of T_x coil will also intersect the R_x coil. The resulting EMF in the R_x coil with N_2 turns is as follows:

$$e.m.f. = -N_2\frac{d\phi_{21}}{dt} = -N_2\frac{d}{dt}(\vec{B_1}\cdot A_2) \tag{1}$$

Assuming that a is the radius of the coil, and z is the axial distance from the center of the T_x coil, the magnetic field strength at the receiver coil depends on the relative magnetic permeability of the medium μ_r, and can be represented as:

$$\vec{B} = [\mu_o\mu_r N_1 a^2 I_1]/[2(a^2+z^2)^{\frac{3}{2}}] \tag{2}$$

While the galvanic coupling offers interference-free communication, the intra-body network may benefit from the MR coupling in multiple aspects. Firstly, the use of a magnetic field can maintain lower path loss in biological tissue since the magnetic permeability of the biological tissue is similar to that for the air [22], which is a distinct benefit than the other two common HBC methods (i.e., galvanic and capacitive couplings). Secondly, the MR coupling method is not affected by the surrounding environment and can communicate without an external reference [29]. Moreover, MR coupling technique does not require a ground plate, which makes it more suitable for implantable application The resonant coupling mode (instead of inductive coupling) maximizes the transmission distance while minimizing the path loss, resembling the resonant wireless power transfer systems [30]. Finally, the transmission signal primarily remains in the magnetic near field and thus limits RF radiation ensuring maximum signal is delivered to the coupled receiver through the body. These advantages consequently reduce the overall power consumption in the HBC systems.

III. Experiment Setup

A. Instruments

A two-port vector network analyzer (VNA; E5061B, Keysight Tech.) was used to measure the S21 parameter, which is the power transfer ratio between port 1 (T_x) and port 2 (R_x). To determine the signal attenuation (or path loss) of galvanic and magnetic resonance couplings, we connected electrodes (for galvanic) or coils (for MR) to the VNA. The transmission frequency range was set between 500 kHz to 160 MHz, and the transmission power was maintained at 0 dBm (1 mW) throughout the study. The measurement device was carefully calibrated before each experiment to ensure accurate measurements. Figs. 2 and 3 show different coupling methods pictorially.

For the galvanic coupling experiments (section IV-A), each T_x and R_x electrode consists of two half-circular (width = 1.6 mm, dia = 33.2 mm, thickness = 0.1 mm) conductive copper sheets (positive and negative electrodes) forming a ring with electrical isolation in the middle (same diameter as the MR coils). The galvanic electrodes were attached to the skin directly with bio-compatible polypropylene film based pressure sensitive adhesive (PSA) tape (ARseal 90880, Adhesives Research) after applying the electrode gel (Spectra 360, Parker Laboratories) to increase the conductivity and eliminate air gaps.

For the capacitive coupling experiments (section IV-A), each T_{x+} and R_{x+} (positive) electrode was made using a conductive copper ring (width = 1.6 mm, dia = 33.2 mm, thickness = 0.1 mm) as shown in Fig. 3(b). Each T_{x-} and R_{x-} (negative) electrode was connected to two separate copper sheets (10 cm $\times$ 3 cm) and placed on insulated platforms 10 cm above the ground to create ground coupling through ground capacitance.

Decoupling the ground between the T_x and R_x was done by utilizing independent test equipment: T_x was connected to a wave generator (4065, BK Precision) while the R_x was connected to an oscilloscope (MSOX 3024T, Keysight Inc.), which were operated using isolated portable power supplies. The channel gain was calculated by measuring the ratio between the voltages across the T_x and R_x using the formula: $P(dB) = 20 \cdot log_{10}(Receiver\ voltage/Transmitter\ voltage)$. The test subjects were also standing on an insulated platform, 1 cm above the ground. The polyimide insulated T_{x+} and R_{x+} electrodes were attached to the forearms and created a capacitive coupling with the body as shown in (Fig. 3(a)).

For the MR coupling experiments (section IV-A - IV-F), we primarily used commercially available RFID coils (Zycoil Electronic Co.) coupled with a capacitor as T_x and R_x. It is a planar coil with 9.27 μH of inductance (made out of 10 turns of 34 AWG, polyimide insulated copper wire, dia = 33.2 mm) connected in parallel with a 14.86 pF capacitor, forming an LC circuit with a resonance frequency of 13.56 MHz. The capacitor values were varied on both T_x and R_x to create resonance at different frequencies. We also used two other MR coil pairs in this study (reported in section IV-B, Fig. 4) which are hand-wound coil (950 nH, 26 AWG, 2 loops, 48 mm diameter), and commercially available chip inductor coil (15 nH, B82422, TDK-EPC Corp.) with corresponding capacitors to create different resonance frequencies.

For the experiment with multiple MR receiver coils (section IV-F) to measure the received power, the voltages (V) across the receiver MR coils were measured using a four-

channel oscilloscope (MSOX 3024T, Keysight Inc.), and the received power was calculated using the formula, $P(dBm) = 10 \cdot log_{10}[P(mW)/1mW]$, where, $P(mW) = V^2/R$, and R is the probe resistance of the oscilloscope (1 $M\Omega$). The transmitter and receiver coils were covered by a specialized magnetic shielding film (WMF200, Woremor) to minimize magnetic interference from nearby electronic equipment and over-the-air transmission [31]. The magnetic shield used in this experiment has $\geq$ 40 dB electromagnetic attenuation for the signal frequency range used in this study.

We also measured the magnetic flux density (Table I) produced by the coils using a magnetic tunnel junction (MTJ) sensor (STJ-240, Micro Magnetics), combined with a Wheatstone bridge circuit and a high-speed digital multimeter (2700, Keithley Instruments). The sensor works by changing its resistance when exposed to a magnetic field, which is converted to magnetic flux density (μT). The ultra-sensitive response of the sensor (1.15%/Oe) can be useful when measuring weaker magnetic fields produced by smaller coils (i.e., MR coil with chip inductor). The Wheatstone bridge provides a more accurate reading of the unknown resistance values from the sensor. It is worth mentioning that the proposed MR coupling requires no metal-free environment. A study by Gulati et al., concluded that having shielding (i.e., aluminum foil) wrapped around the transmitter or placing a strong magnet near the transmitter did not significantly perturb the magnetic communication [32]. The magnetic field produced by our MR coupling method was below 1 μT, which can provide longer and better communication links without direct current flow through the body. The study by Ogasawara et al. on the effect of magnetic coupling also presented a similar conclusion [18].

B. Experimental protocol with human subjects

All experiments in this study were conducted on human volunteers. The experimental methods were approved by Temple University's institutional review board (IRB). Seven healthy adult participants (5 males and 2 females) were selected for the study (age: 21-65 years). The IBNet transmission measurements were taken on all volunteers across different body parts (i.e., hand, arm, chest, waist, thigh, calf, shoulder, etc.) on a ground isolated platform while standing and in other postures. Since the transmitted power was well below the safety thresholds, no adverse impacts were expected and the subjects did not feel any effect during the experiments [33]–[35].

C. Safety considerations

Unregulated exposure to non-static electromagnetic fields over extended time may cause adverse health effects on humans [35]. In this study, we strictly maintained the electrical transmission power output at 0 dBm (1 mW) from the vector network analyzer. The maximum magnetic flux density generated from the coils was below 1 μT (Table: I), well under the reported safety threshold limit according to the IEEE standard for safety levels with respect to human exposure to magnetic fields [34] for our operating frequency range 500 kHz to 160 MHz. No sensation was reported throughout the duration of this study as the transmitted power was too low to be felt, or cause any localized heating, or cause any absorption by the tissue.

IV. Results and Discussion

A. MR coupling vs. other coupling methods

In order to validate the MR coupling provides a better signal transmission performance than other methods for IBNet, we measured the channel gain (dB) using a pair of galvanic electrodes, a pair of capacitive electrodes, and a pair of MR coupling coils on the forearms of a human volunteer (Fig. 3(a)). The probes (electrodes and coils) are shown in Fig. 3(b). The distance between the probes through the body was maintained at 100 cm. As for the MR coupling, we also placed the MR coils at 100 cm distance in air (parallel to each other) to observe the transmission performance in the air. Using the VNA, we measured the channel gain (dB) from 500 kHz to 160 MHz. Fig. 3(c) shows that MR coupling in the body demonstrated the highest channel gain at least up to 15 MHz, which is in good agreement with the literature [29].

However, as the frequency increases above ~15 MHz, the signal begins transitioning from magnetic induction to the RF radiation [36], which experienced channel gain drops. It is attributed to high water content in the human body ($\geq$ 60%) that blocks RF well (this is known as the shadowing effect). This effect leads to a higher signal attenuation at high frequency for RF signal in the body [37], [38]. However, the higher frequency signal may also radiate through the air instead of the body in form of electromagnetic (EM) waves. This leads to some improvement in the gain after around 25-35 MHz. It is even prominent around $\geq$ 60 MHz, where the performance of all three methods is almost the same.

Human body tissues are dominantly diamagnetic and are not affected by typical magnetic fields ($\mu_r \approx 1$) [39]. The magnetic field from the coils that propagates through the body is similar to the propagation if it were in the air. However, the MR coupling mode worked significantly better in the human body, compared to that through the air, at the given distance because the attenuation through the body is found to be significantly lower ($20 \leq PL \leq 55$ dB). It is attributed to the far field components in the body favoring the intra-body transmission. Recently, Park et al. [40] reported that such far-field effects are observed due to the higher relative permittivity of human tissue ($\varepsilon_r \approx 11$ - 464 as compared to ≈ 1.0 in the air) [41]. The relative permittivity effectively reduces the wavelength using the following equation, $\lambda_m = \lambda/\sqrt{\varepsilon_r}$, where λ_m is the wavelength in the medium of relative permittivity ε_r [42]. For example, the wavelength for a 13.56 MHz signal in the muscle tissue ($\varepsilon_r = 152$) will be reduced to 1.8 meters from 22 meters. Therefore, the near field region boundary ($\lambda_m/2\pi$) is reduced in the tissue, and the far field radiation is enhanced, which has a lower attenuation factor contributing to a significant improvement in the transmission.

B. Performance comparison using different MR coils

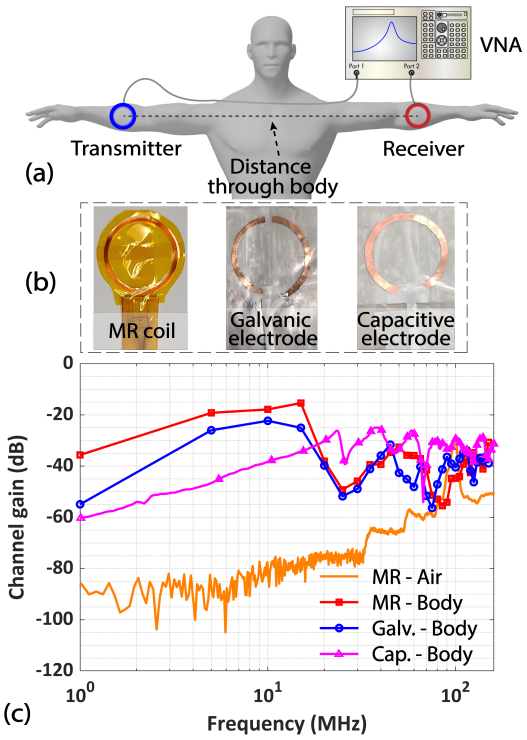

Fig. 3. (a) $\boldsymbol{T_x}$ and $\boldsymbol{R_x}$ probe placements on the body; (b) MR coil, galvanic electrode, and capacitive electrode; (c) comparison of channel gain using different coupling methods.

After confirming that MR coupling provides comparatively better performance, we investigated how the coil design affects the signal transmission performance. Considering the magnetic flux density, inductance, and mutual coupling factor, we selected three different MR coils (Fig. 4(a-c)). For this experiment, we set the resonance frequency for all coils at 13.56 MHz since we observed the least path loss at resonance as shown in Fig. 3(c); it is also similar to the commercial RFID coil. The design specifications for the coils are provided in Table I). The T_x and R_x probes were placed in the forearms of a human subject and covered by the magnetic shielding films (Fig. 3(a)). The channel gain (dB) was measured from 500 kHz to 160 MHz. As shown in Fig. 4(d), the experimental results show that the MR coil with the highest magnetic flux density (33.2 mm coil) resulted in overall the best transmission performance with the lowest transmission loss at the resonance frequency. Additional experiments were carried out to demonstrate the dependency of the diameter of the coils (keeping N = 10) with the channel gain performance. The results are shown in Fig. S1, in the supplementary document. The experiment shows higher diameter coil performed better, therefore, it could be concluded that the best performing coil needs to be selected based on the coil diameter and number of turns which will introduce a tradeoff between the performance and the dimension of the coils for implantable systems. The coil dimension for implantable applications needs to be carefully selected after these considerations. Although the majority of channel gain was near the resonance frequency, the MR coils also showed an improvement in the higher frequency region ($\geq$ 25 MHz). This increase could be associated with the RF radiation from the coils, which initiates data transmission through the air along with the body [43]. Since 33.2 mm MR coil (N = 10) performed the best at its resonance frequency out of these three distinctive coil dimensions (Fig. 4(d)), we choose to continue the subsequent experiments in this study with this coil at 13.56 MHz resonance frequency.

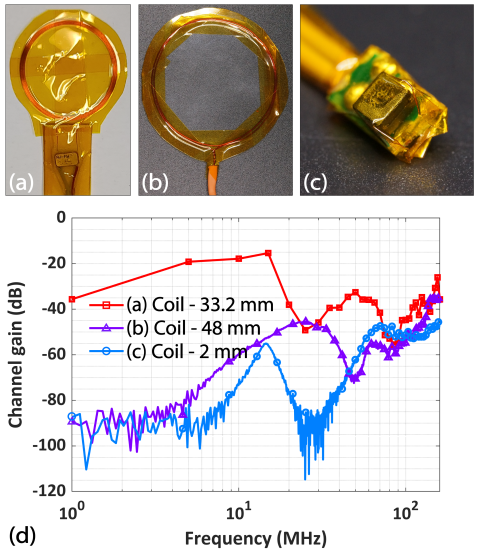

Fig. 4. Three MR coil performance compared: (a) coil - 33.2 mm, (b) coil - 48 mm, (c) coil - 2 mm, and (d) channel gain performance.

TABLE I
MR COIL SPECIFICATIONS (RESONANCE FREQUENCY = 13.56 MHZ)

Parameter	Coil type - 1	Coil type - 2	Coil type - 3
1. Dimension	Dia = 33.2 mm N = 10 turns	Dia = 48 mm N = 2 turns	L = 3.2 mm W = 2.0 mm
2. Inductance	9.27 μH	950 nH	15 nH
3. Capacitance	14.86 pF	145 pF	9.2 nF
4. Magnetic flux density	0.962 $\pm$ 0.01 μT	0.224 $\pm$ 0.001 μT	0.074 $\pm$ 0.004 μT

C. MR path loss through human body

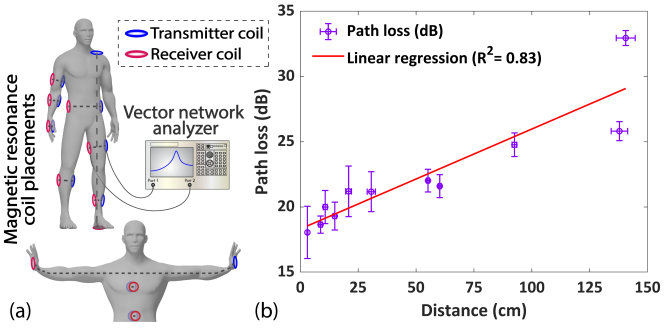

Fig. 5. (a) MR coil placement on human body for direct transmission measurement; (b) Path loss in human body with MR coupling ($\boldsymbol{F_r = 13.56\ MHz}$).

Next, the comprehensive MR coupling path loss over the human body was studied. In these experiments, T_x and R_x probes were placed parallel to each other at different parts of the body as shown in Fig. 5(a) and connected to the VNA.

Fig. 5(b) shows the measured path loss over different distances between the T_x and R_x coil pair from human subjects. The path loss was measured through the hand, forearm, arm, lower calf, calf, chest to back, thigh, belly, hips, shoulder to feet, and left hand palm to right hand palm. As seen, the path loss increased almost linearly with distance (R^2 = 0.83). The minimum path loss was measured through hand (18.05 $\pm$ 4.01 dB) for the minimum distance (3.08 $\pm$ 0.45 cm). The maximum path loss was measured through the left hand to the right hand (32.95 $\pm$ 1.14 dB) for maximum distance (140.57 $\pm$ 8.22 cm). The path loss between left to right hand was significantly higher than the path loss between shoulder to heel ($\sim$ 7.14 dB increase) although the distance was only increased by a couple of centimeters on average. It may attribute to the fact that the bone to tissue volume ratio on hands is generally much higher than that of the rest of the body [44], [45]. Although the magnetic permeability of biological tissues is similar to the magnetic permeability in free space [22], the permittivity (F/m), conductivity (S/m) are significantly lower in bone compared to skin, fat, and muscle tissue; thus the overall loss of the signal is shown to be higher in this path [46]–[48]). For other locations in the body, the effect of bone was less significant due to shorter travel path through the body (i.e., arm, lower calf, chest to back, etc.). Linear regression between those data points (excluding left hand to right hand) yields a more linear (R^2 = 0.91) fitting of the regression line with an estimated 0.0547 dB/cm + 18.88 dB path loss.

D. Effect of transceiver alignment on human body

1) Angular position at adjacent distances: In theory, the best transmission between the T_x and R_x coils occurs when they are parallel to each other, but keeping them parallel in intra or on-body scenarios is a challenge. For this, we placed the receiver coil on the opposite side of the body locations (i.e., arm, waist, thigh, and calf) for 0° misalignment and on the right angle side for 90° misalignment, as shown in Fig. 6(a). The measured path loss comparing 0° and 90° misalignment for each location is shown in Fig. 6(b). We observed that the 90° misalignment performed slightly worse in path loss for most cases (except for the arm), but the differences were nearly negligible; the difference in average path loss was less than 0.33 dB. Thus, we conclude that the angular misalignment of T_x and R_x coils does not affect much, which makes the MR coupling even more attractive for IBNet.

2) Angular position at remote distances: Next, we examined if angular misalignment at a longer distance still provides a reasonable path loss. For this experiment, we attached the transmitter coil on the shoulder of the volunteers and attached the receiver coil at three different body locations (waist, thigh, and calf) at approximately 90° misalignment as shown in Fig. 7(a). The measured path loss was 20.81 $\pm$ 1.50 dB at waist (distance = 39.74 $\pm$ 3.97 cm), 21.20 $\pm$ 1.94 dB at thigh (distance = 73.43 $\pm$ 5.86 cm), and 22.80 $\pm$ 2.56 dB at calf (distance = 106 $\pm$ 4.76 cm) as shown in Fig. 7(b). The results are very close to the path loss measured at similar distances when the T_x and R_x were aligned with each other (Fig. 5(b)).

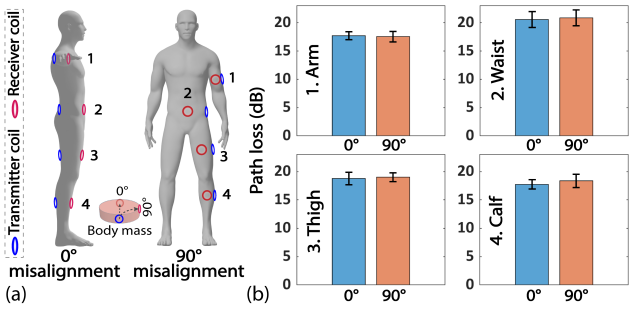

Fig. 6. (a) Experiment setup for angular misalignment of T_x-R_x in adjacent location; (b) performance of angular misalignment in adjacent location on the human body.

It can be concluded that the misalignment does not matter much even at longer distances.

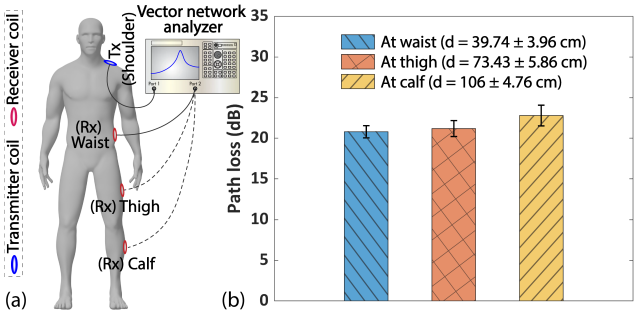

Fig. 7. (a) Experiment setup for angular misalignment of T_x-R_x in distant location; (b) performance of angular misalignment in distant location on the human body.

E. Path loss due to different postures

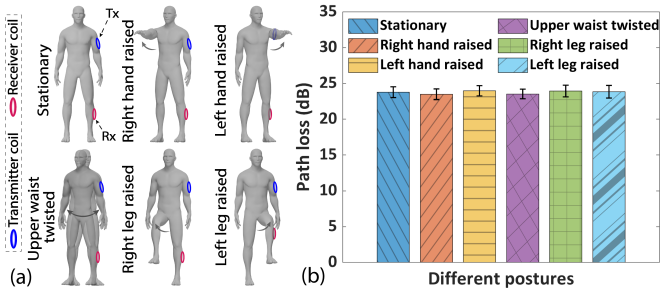

Fig. 8. (a) Different postures; (b) corresponding transmission performance.

We have also investigated if body movement will have any adverse effects on effective path loss. For this experiment, the transmitter MR coil was attached to the left arm of the volunteers and the receiver MR coil was attached to the calf on the same side. The direct distance through the tissue between the T_x and R_x coils were in a range of 80 to 112 cm depending on the subjects (the in-air distance range was 63 to 95 cm). The volunteers were asked to maintain different postures during the experiment as shown in Fig. 8(a). During these postures, the skin and muscle around the arm and calf contracted or expanded which had some minor effects on the measured path loss. The path loss data were recorded and shown in Fig. 8(b).

Since our choice of communication frequency was 13.56 MHz and the coils were covered by shielding film (section III-A) to prevent electromagnetic radiation, the measured path loss was entirely through the body. In summary, the path loss due to different postures had an average of 23.76 $\pm$ 0.21 dB, 95 % confidence interval [CI], and thus showed minimal effect due to posture or movement.

F. Multi-node receiver in magnetic resonance coupling

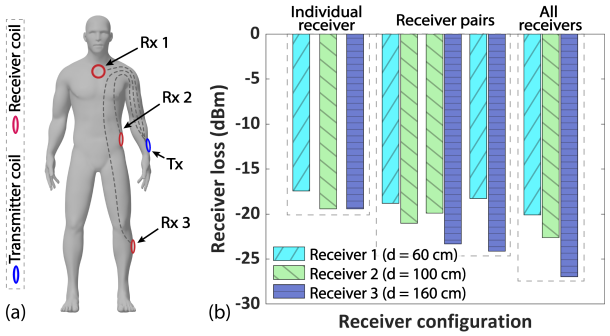

Fig. 9. (a) Three MR receivers placed on a body at different distances ($\boldsymbol{T_x}$ on wrist and, $\boldsymbol{R_x}$s on chest, waist, and calf); (b) receiver loss measured with a different number of receivers activated at the same time ($P_{\boldsymbol{Tx}} = \boldsymbol{0\ dBm}$).

To investigate how well signal (power/data) can be delivered to multiple wearable devices, an experiment was performed where we placed a single transmitter coil on the wrist and multiple receiver coils on the chest, waist, and calf of the volunteers. Corresponding average distance between the T_x and R_x was about 60, 100, and 160 cm respectively as shown in Fig. 9(a). A three-receiver system has seven independent configurations where one or multiple receivers are activated at a time. Since transmitted power is fixed, when the number of the receiver increases, the transmitted power is shared, and the power received by individual R_x probe is reduced compared to the power they receive when working exclusively. The receiver loss in terms of dBm is shown in Fig. 9(b) and summarized in Table II.

TABLE II
MULTI RECEIVER POWER SHARING
($\boldsymbol{P_{Tx} = 0\ dBm,\ F_r = 13.56\ MHz}$)

Active receiver(s)	P_{Rx_1} (dBm)	P_{Rx_2} (dBm)	P_{Rx_3} (dBm)	Total (dBm)
1. R_{x1}	-17.43			-17.43
2. R_{x2}		-19.41		-19.41
3. R_{x3}			-19.41	-19.41
4. R_{x1} + R_{x2}	-18.80	-21.03		-16.77
5. R_{x2} + R_{x3}		-19.90	-23.31	-18.27
6. R_{x1} + R_{x3}	-18.27		-24.12	-17.27
7. R_{x1} + R_{x2} + R_{x3}	-20.10	-22.63	-26.97	-17.63

Maximum -17.43 dBm receiver loss was observed at the closest receiver R_{x1} at 60 cm distance when it was working independently and maximum -16.77 dBm combined receiver loss was observed when R_{x1} and R_{x2} were simultaneously active. It indicates that having multiple receivers may increase the overall efficiency of the transmission by capturing more electromagnetic fields at the area of placement. However, there will be a limitation on how many receivers can be added based on the receiver positions, gain, path loss, and transmitted power. Additionally, advanced algorithms can be employed to control the activity schedule of the receivers to increase the overall efficiency of the transmission [49].

These experiments demonstrate that MR path loss through the body is not only lower than other methods, but also rather insensitive with respect to the coil orientations, body posture, and movement. This makes MR quite an attractive technology for IBNet use.

V. Conclusion

Traditional means of intra-body communication (i.e., galvanic, capacitive, RF) for IBNet are affected by many factors such as higher path loss due to tissue absorption, shadowing effect, environmental variations, instability of the quality of transmission, grounding issues, antenna size, etc. We have demonstrated that the MR coupling is comparatively much more robust and yet shows a lower path loss, and thus is better suited for IBNet. We have also observed that the transmission is not affected much by the angular position of the transmitter or receiver coils, the movement or posture also did not show any significant impact proving its viability for implantable and wearable devices. Additionally, multi-receiver experiments have shown that a multi-node sensor communication system can also be created. Overall, the MR coupling method enables conserving energy for long-term implants by enabling low power communication at lower path loss in the human body.

Our evaluation, however, encountered several difficulties. For example, it was quite difficult to obtain exactly the same resonance frequency for both T_x and R_x coils due to slight mismatches in the component values. Another issue was the effect of body impedance on the transmission signal, which would require further study. In particular, it is also important to understand the packet error rates in different parts of the body and at different distances and what kind of encoding schemes could reduce it. This work is currently underway and will be reported in future papers.

Acknowledgment

The authors would like to acknowledge John Arthur Papacostas, Rebecca Campbell, and Abdulaziz Almeseri from Temple University for their help with the experiments.

References

[1] W. M. Chardack, A. A. Gage, and W. Greatbatch, "A transistorized, self-contained, implantable pacemaker for the long-term correction of complete heart block." *Surgery*, vol. 48, pp. 643–54, oct 1960.

[2] H. Y. Tung, K. F. Tsang, H. C. Tung, K. T. Chui, and H. R. Chi, "The design of dual radio zigbee homecare gateway for remote patient monitoring," *IEEE Transactions on Consumer Electronics*, vol. 59, no. 4, pp. 756–764, 2013.

[3] H. Tung, K. Tsang, K. Lam, H. Tung, B. Li, L. Yeung, K. Ko, W. Lau, and V. Rakocevic, "A mobility enabled inpatient monitoring system using a zigbee medical sensor network," *Sensors*, vol. 14, no. 2, pp. 2397–2416, jan 2014.

[4] T. M. Bruns, N. Bhadra, and K. J. Gustafson, "Bursting stimulation of proximal urethral afferents improves bladder pressures and voiding," *Journal of neural engineering*, vol. 6, no. 6, p. 066006, 2009.

[5] A. Mendez, M. Sawan, T. Minagawa, and J.-J. Wyndaele, "Estimation of bladder volume from afferent neural activity," *IEEE Transactions on Neural Systems and Rehabilitation Engineering*, vol. 21, no. 5, pp. 704–715, 2013.

[6] C. Powell, "Conditional electrical stimulation in animal and human models for neurogenic bladder: working toward a neuroprosthesis," *Current bladder dysfunction reports*, vol. 11, no. 4, pp. 379–385, 2016.

[7] R. G. HAUSER, "Techniques for improving cardiac performance with implantable devices," *Pacing and Clinical Electrophysiology*, vol. 7, no. 6, pp. 1234–1239, 1984.

[8] K. Kaszala and K. A. Ellenbogen, "Device sensing: sensors and algorithms for pacemakers and implantable cardioverter defibrillators," *Circulation*, vol. 122, no. 13, pp. 1328–1340, 2010.

[9] R. A. Normann and E. Fernandez, "Clinical applications of penetrating neural interfaces and utah electrode array technologies," *Journal of neural engineering*, vol. 13, no. 6, p. 061003, 2016.

[10] A. Celik, K. N. Salama, and A. Eltawil, "The internet of bodies: A systematic survey on propagation characterization and channel modeling," 9 2020. [Online]. Available: https://doi.org/10.36227/techrxiv.12912752.v2

[11] D. Werber, A. Schwentner, and E. M. Biebl, "Investigation of RF transmission properties of human tissues," *Advances in Radio Science*, vol. 4, no. 4, pp. 357–360, sep 2006.

[12] H.-Z. T. Chen and A. S.-L. Lou, "A study of rf power attenuation in bio-tissues," *Journal of Medical and Biological Engineering*, vol. 24, no. 3, pp. 141–146, 2004.

[13] X. fang Li and S. Zhang, "Galvanic coupling type intra-body communication human body implantable sensor network," in *Advances in Intelligent and Soft Computing*. Springer Berlin Heidelberg, 2012, pp. 147–152.

[14] W. J. Tomlinson, K. R. Chowdhury, and C. Yu, "Galvanic coupling intra-body communication link for real-time channel assessment," in *IEEE INFOCOM Workshops*. IEEE, Apr. 2016.

[15] Y. Xu, Z. Huang, S. Yang, Z. Wang, B. Yang, and Y. Li, "Modeling and Characterization of Capacitive Coupling Intrabody Communication in an In-Vehicle Scenario," *Sensors*, vol. 19, no. 19, p. 4305, oct 2019.

[16] A. Datta, M. Nath, D. Yang, and S. Sen, "Advanced Biophysical Model to Capture Channel Variability for EQS Capacitive HBC," *IEEE Transactions on Biomedical Engineering*, 2021.

[17] Y. K. Hernandez-Gomez, G. A. Alvarez-Botero, J. B. Rodriguez, and F. R. de Sousa, "Magnetic human body communication based on double-inductor coupling," in *IEEE I2MTC*, vol. 9, 2017, pp. 1–6.

[18] T. Ogasawara, A. I. Sasaki, K. Fujii, and H. Morimura, "Human body communication based on magnetic coupling," *IEEE Transactions on Antennas and Propagation*, vol. 62, no. 2, pp. 804–813, 2014.

[19] S. Banou, K. Li, and K. Chowdhury, "MAGIC: Magnetic Resonant Coupling for Intra-body Communication," in *IEEE INFOCOM 2020 - IEEE Conference on Computer Communications*, vol. 2020-July. IEEE, jul 2020, pp. 1549–1558.

[20] R. Zhang, H. Liu, Q. Shao, G. Li, X. Fang, and H. Li, "Effects of Wireless Power Transfer on Capacitive Coupling Human Body Communication," *IEEE/ASME Transactions on Mechatronics*, vol. 20, no. 3, pp. 1440–1447, jun 2015.

[21] M. S. Wegmueller, M. Oberle, N. Felber, N. Kuster, and W. Fichtner, "Signal transmission by galvanic coupling through the human body," *IEEE Transactions on Instrumentation and Measurement*, vol. 59, no. 4, pp. 963–969, 2010.

[22] M.-R. Tofighi, "Interaction between electromagnetic waves and biological materials," in *Principles and Applications of RF/Microwave in Healthcare and Biosensing*. Elsevier, 2017, pp. 53–101.

[23] B. Kibret, M. Seyedi, D. T. H. Lai, and M. Faulkner, "Investigation of galvanic-coupled intrabody communication using the human body circuit model," *IEEE Journal of Biomedical and Health Informatics*, vol. 18, no. 4, pp. 1196–1206, 2014.

[24] N. Cho, J. Yoo, S. Song, J. Lee, S. Jeon, and H. Yoo, "The human body characteristics as a signal transmission medium for intrabody communication," *IEEE Transactions on Microwave Theory and Techniques*, vol. 55, pp. 1080–1086, 2007.

[25] J. Bae, H. Cho, K. Song, H. Lee, and H.-J. Yoo, "The signal transmission mechanism on the surface of human body for body channel communication," *IEEE Transactions on Microwave Theory and Techniques*, vol. 60, no. 3, pp. 582–593, 2012.

[26] S. Maity, M. He, M. Nath, D. Das, B. Chatterjee, and S. Sen, "Bio-physical modeling, characterization, and optimization of electro-quasistatic human body communication," *IEEE Transactions on Biomedical Engineering*, vol. 66, no. 6, pp. 1791–1802, jun 2019.

[27] M. H. Seyedi and D. Lai, *A Novel Intrabody Communication Transceiver for Biomedical Applications*, ser. Series in BioEngineering. Singapore: Springer Singapore, 2017.

[28] T. G. Zimmerman, "Personal area networks: Near-field intrabody communication," *IBM Systems Journal*, vol. 35, no. 3.4, pp. 609–617, 1996.

[29] J. Park and P. P. Mercier, "Magnetic human body communication," *Proceedings of the Annual International Conference of the IEEE Engineering in Medicine and Biology Society, EMBS*, vol. 2015-Novem, pp. 1841–1844, 2015.

[30] B. L. Cannon, J. F. Hoburg, D. D. Stancil, and S. C. Goldstein, "Magnetic resonant coupling as a potential means for wireless power transfer to multiple small receivers," *IEEE Transactions on Power Electronics*, vol. 24, no. 7, pp. 1819–1825, 2009.

[31] M. Bailleul, "Shielding of the electromagnetic field of a coplanar waveguide by a metal film: Implications for broadband ferromagnetic resonance measurements," *Applied Physics Letters*, vol. 103, no. 19, Nov. 2013.

[32] R. K. Gulati, A. Pal, and K. Kant, "Experimental Evaluation of a Near-Field Magnetic Induction Based Communication System," in *2019 IEEE Wireless Communications and Networking Conference (WCNC)*, vol. 2019-April. IEEE, apr 2019, pp. 1–6.

[33] K. Mizuno, N. Shinohara, and J. Miyakoshi, "In vitro evaluation of genotoxic effects under magnetic resonant coupling wireless power transfer," *International Journal of Environmental Research and Public Health*, vol. 12, no. 4, pp. 3853–3863, Apr. 2015.

[34] "IEEE standard for safety levels with respect to human exposure to electric, magnetic, and electromagnetic fields, 0 hz to 300 GHz," 2019.

[35] "Guidelines for limiting exposure to time-varying electric and magnetic fields (1 Hz TO 100 kHz)," International Commission on Non-Ionizing Radiation Protection, Tech. Rep. 6, 2010.

[36] A. Pal and K. Kant, "Nfmi: Near field magnetic induction based communication," *Computer Networks*, vol. 181, no. July, p. 107548, nov 2020.

[37] J. F. Zhao, X. M. Chen, B. D. Liang, and Q. X. Chen, "A review on human body communication: signal propagation model, communication performance, and experimental issues," *Wireless Comm. and Mobile Comp.*, vol. 2017, 2017.

[38] M. Synthia, "Impacts of human body shadowing in wireless body-centric communications," *International Journal of Future Generation Communication and Networking*, vol. 9, no. 6, pp. 191–200, Jun. 2016.

[39] H. Scharfetter, R. Casanas, and J. Rosell, "Biological tissue characterization by magnetic induction spectroscopy (MIS): requirements and limitations," *IEEE Transactions on Biomedical Engineering*, vol. 50, no. 7, pp. 870–880, Jul. 2003.

[40] J. Park and P. P. Mercier, "A sub-10-pj/bit 5-mb/s magnetic human body communication transceiver," *IEEE Journal of Solid-State Circuits*, vol. 54, no. 11, pp. 3031–3042, 2019.

[41] R. Pethig, "Dielectric properties of biological materials: Biophysical and medical applications," *IEEE Transactions on Electrical Insulation*, vol. EI-19, no. 5, pp. 453–474, 1984.

[42] T. K. Wotherspoon and M. Higgins, "Implantable wireless body area networks," in *Implantable sensor systems for medical applications*, A. Inmann and D. Hodgins, Eds. Elsevier, 2013, ch. 14.

[43] Ž. Lucev, I. Krois, and M. Cifrek, "A Capacitive Intrabody Communication Channel from 100 kHz to 100 MHz," *IEEE Transactions on Instrumentation and Measurement*, vol. 61, no. 12, pp. 3280–3289, dec 2012.

[44] J. C. Cianca and S. I. Patel, *Musculoskeletal Ultrasound Cross-Sectional Anatomy*, vol. 148.

[45] A. Rad, "Cross sectional anatomy," 2021. [Online]. Available: https://www.kenhub.com/en/library/anatomy/cross-sectional-anatomy

[46] D. Andreuccetti, R. Fossi, and C. Petrucci, "Dielectric Properties of Body Tissues."

[47] M. Wolf, R. Gulich, P. Lunkenheimer, and A. Loidl, "Broadband dielectric spectroscopy on human blood," *Biochimica et Biophysica Acta (BBA) - General Subjects*, vol. 1810, no. 8, pp. 727–740, 2011.

[48] E. Levy, M. David, G. Barshtein, S. Yedgar, L. Livshits, P. Ben Ishai, and Y. Feldman, "Dielectric response of cytoplasmic water and its connection to the vitality of human red blood cells. ii. the influence of storage," *The Journal of Physical Chemistry B*, vol. 121, no. 20, pp. 5273–5278, 2017, pMID: 28453275.

[49] J. Zhang, S. Zheng, T. Zhang, M. Wang, and Z. Li, "Charge-aware duty cycling methods for wireless systems under energy harvesting heterogeneity," *ACM Transactions on Sensor Networks*, vol. 16, no. 2, 2020.